Design and testing of a self-centering friction damper-brace for compression ultimate limit state: Inelastic buckling

Seyed Mohamad Mahdi Yousef-beik [a], Sajad Veismoradi [a,*], Pouyan Zarnani [a], Pierre Quenneville [b]

[a] *Department of Built Environment Engineering, School of Future Environments, Auckland University of Technology, Auckland, New Zealand*
[b] *Department of Civil and Environmental Engineering, Faculty of Engineering, The University of Auckland, Auckland, New Zealand*

A B S T R A C T

This paper investigates the design procedures and experimental testing of a low-damage brace equipped self-centering friction-based connection named Resilient Slip friction Joint (RSFJ). The brace energy dissipation and restoring force is provided by the damper component. Previous studies have shown that the damper ultimate compression strength might be jeopardized due to damper rotational flexibility, which might lead to premature elastic buckling of the brace. To address the issue, a concept of telescopic tubes was introduced to be put in parallel to the damper(s). The design of the telescopic tube requires a thorough framework that considers different possible failure loads and the collapse modes, so that the brace ultimate strength can be accurately estimated. Such a process tends to be more complex than the conventional Concentrically Braced Frames (CBFs), due to the non-continuity(ies) appearing as damper installation which may lead to possible plastic hinge formation in different locations of the brace. This study aims to employ second-order plastic analysis for the design of the damper-brace assembly. The proposed method is, is then validated with current international codes' procedure and also with destructive tests on the self-centring brace specimens. Finally, the seismic design considerations including the design of the connections and protected members are discussed in this paper. The current procedure could also be recruited for other new emerging damper-braces as well.

1. Introduction

In an attempt to increase the disaster-resiliency of the structures against seismic hazards, self-centring low-damage structures have been developed with the main intention of providing damage-avoidant and/or replaceable seismic fuses [1]. Priestley et al. [2] started to study the performance of these system in the late nineteen century through the program entitled "Pre-cast Seismic Structural Systems or PRESSS". In this program, the post-tensioned cables were used with dampers to bring the flag-shape hysteresis performance. The extension of the concept to the braced frame structures was proposed by Christopoulos et al. [3] where they developed a new self-centring energy dissipative brace using two hollow steel box sections, post-tensioned tendons and friction dampers. In this regard, several researchers have also studied and developed self-centring braces but with different mechanism of re-centring and sources of damping [4–14]. Structural application of friction dampers was firstly demonstrated for the steel braced frames in

the early 1980 [15,16], which was followed by the generalization to the Moment-Resisting Frames (MRF) by Popov et al. [17] and Clifton et al. [18]. The self-centring friction dampers (Called Ringfeder) was firstly studied and tested by Nims et al. [19] and Filiatrault et al. [20] and then it founds it way to building industry [13,14,21,22]. For more information regarding the friction dampers, readers are referred to [23–25]. The Resilient slip friction joint (RSFJ) is an elevated version of Ringfeder dampers, which was originally developed by Zarnani and Quenneville in 2015 [26] and extended to different lateral load resisting systems including the self-centring tension-compression braces [27–31], self-centring tension-only braces [32,33], rocking timber or concrete shear walls [34,35], rocking steel braced frames with shear links [36], retrofitting of brittle structures [37,38] and rotational links [39,40].

RSFJ tension-compression brace assembly is composed of three main elements as depicted in Fig. 1. The first element is the damper, which depending on the displacement demand can be installed in either one or two locations along with the brace (Fig. 1.a or Fig. 1.b). The second
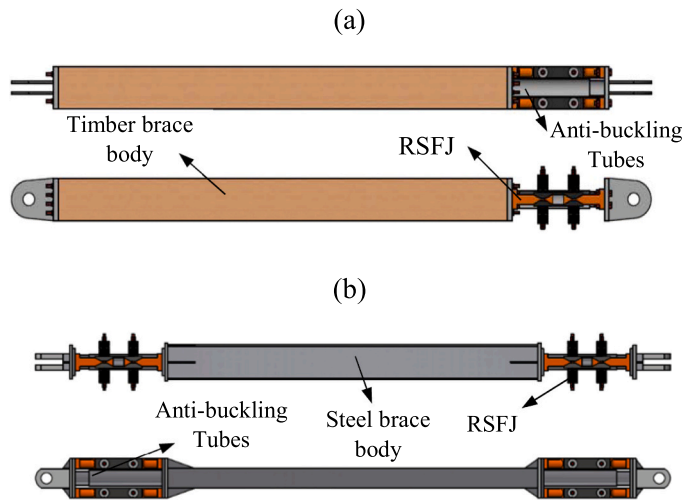
(a)

(b)

Fig. 1. (a) RSFJ brace with one damper and timber brace body [27], (b) RSFJ brace with two dampers and steel body.

element is the brace body, which depending on the architectural or structural considerations can be made up of either timber or steel. The last but not the least element is the telescopic steel tubes entitled "Anti-Buckling Tubes or ABT", which are responsible to strengthen the brace where dampers are located, thereby improving the compressive performance of the brace in terms of postponing the premature instability. Previous studies [27,28,41] demonstrated that if the RSFJ brace is not strengthened with the ABT, the compression capacity of the brace would be very low because of the rotational flexibility of RSFJ [27]. Although the performance has been shown to be improved with ABT installation, yet the ultimate strength (failure load) and failure mode was not carefully investigated. In this regard, the present study attempts to propose a simplified method by which the failure load and collapse mode of the self-centring brace can be predicted. In this process, the method is firstly validated against the current code procedure for quantifying the ultimate strength of the conventional braces and then is authenticated using destructive tests on the self-centring brace specimens.

The problem with the premature inelastic buckling of the brace was also observed for other braces [42–44]. More specifically, for instance, Xu et al. [42] observed the inelastic buckling for a self-centring brace when the axial displacement ratio exceeded 2%, yet the frame work for quantification of the strength was not discussed. The comparable premature instability problem for BRBs (Buckling-Restrained Braces) was studied and reported by Takeuchi et al. [43,44]. In order to quantify the failure mode and ultimate strength of the BRB, they used Simplified Collapse Mechanism Analysis (SCMA) – which will be discussed further in the subsequent section – and advised two stability limits.

2. Simplified collapse mechanism analysis (SCMA)

The behaviour of most of conventional steel braces - with symmetrical cross section - when subjected to a compressive load is shown in Fig. 2 in black continuous line. The lateral deflection (δ) will increase as the axial load (P) grows due second-order ($p - \Delta$) effects, and the rate of this increase will accelerate as the axial load approaches the Euler (elastic) buckling load (P_{cr}) asymptotically. During this travel, a plastic hinge may form at the midspan of the brace due to combined effect of the axial force and the second-order moment. If the brace is stocky (relatively small slenderness ratio $\lambda = L/r$), the plastic hinge will form at a force less than the elastic buckling load (or the lateral displacement at failure point is of small magnitude (Fig. 2.a)). On the contrary, if the brace is slender (relatively large slenderness ratio $\lambda = L/r$), the plastic hinge will form at a force very close to the elastic buckling (or the lateral displacement at failure is of considerable magnitude (Fig. 2.b)). This load at which the brace becomes mechanism and unstable can be regarded as the ultimate strength of the brace and can be well approximated using the "elastic perfectly plastic analysis", which here will be referred to as SCMA – Simplified Collapse Mechanism Analysis.

The basis of this method lies in intersecting two curves namely: (i) stiffness deterioration (shown with ascending blue dash-dot line in Fig. 2) and (ii) strength deterioration (shown with the descending red dash-dot line in Fig. 2). The first curve shows the behaviour of an imperfect brace (with an inherent initial out-of-straightness) in which the axial force tends to converge to the Euler load asymptotically. The reason why it is entitled as *stiffness deterioration* curve is that the system is losing its axial (or lateral) stiffness as approaching the Euler load.

The latter curve shows the decreasing strength of the member (combined action formulae -Eq.2). The reason why it is entitled as *strength deterioration* curve is that the axial strength of the member is deteriorating as the lateral deflection is increasing. It should be noted that if the member is statically determinant, the strength deterioration curve is governed by the section strength mainly because one plastic hinge is needed to be formed to make the system a mechanism. However, if the member is statically indeterminate, the strength deterioration curve should be derived from the plastic analysis involving more plastic hinges to form (See appendix [45]). This is out-of-scope of the current study as the brace is assumed to have a pin-pin connection, and it needs further investigation. In case of a pin-pin brace (determinant system), the strength deterioration curve is shown in Eq.2 –[46]. This method is introduced and employed in the literature as an alternative method for approximating the ultimate strength of the compressive members like columns, CBF braces and BRB braces [43,44,47].

The stiffness deterioration curve can be well approximated using Eq.1 [47], which, in fact, illustrates the impact of second-order actions ($P - \Delta$) on the axial performance:

$$P(\delta) = P_{cr} \frac{\delta}{\delta + \delta_0} \tag{1}$$

where P_{cr} is the elastic or Euler buckling load, δ is the lateral deflection

(a)

(b)

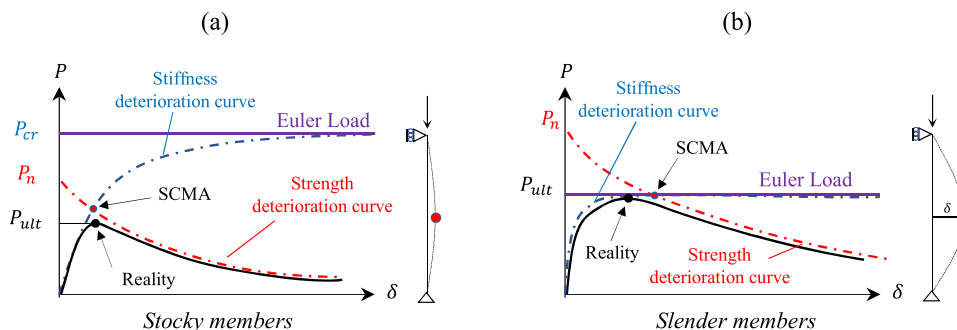**Fig. 2.** performance of the column (steel brace) subjected to compression force (a) stocky members and (b) slender members [47].

at midspan, and δ_0 is the initial-imperfection of the brace at midspan, normally considered to be ($L/1000$). The strength deterioration curve can be approximated conservatively as Eq.2 for determinant system ignoring the variation for different structural shapes [48,49]:

$$\frac{P}{P_n} + \frac{P\delta}{M_p} = 1 \tag{2}$$

where P_n is the squash load and equals the yield stress of the steel multiplied by the gross cross-section area ($A_g F_y$). M_p is the plastic flexural strength of the section ($Z F_y$) assuming that the section is compact enough to develop a perfect plastic behaviour without any prior local instability. If Eq.2 is rearranged, Eq.3 would yield as below:

$$P(\delta) = \frac{M_p}{\frac{M_p}{P_n} + \delta} \tag{3}$$

By intersecting the mentioned two curves (Eq.1 and Eq.3), the lateral deflection at which the plastic mechanism would form (the intersection point - δ_{int}) will be derived as:

$$\delta_{int} = 0.5 M_p \left[\frac{1}{P_{cr}} - \frac{1}{P_n} + \sqrt{\left(\frac{1}{P_{cr}} - \frac{1}{P_n}\right)^2 + \frac{4\delta_0}{M_p P_{cr}}} \right] \tag{4}$$

Finally, the ultimate (collapse) load of the brace can be calculated if the intersection point is input to either of the stiffness or strength deterioration curves as:

$$P_{ult} = P_{cr} \frac{\delta_{int}}{\delta_{int} + \delta_0} \tag{5}$$

Or

$$P_{ult} = \frac{M_p}{\frac{M_p}{P_n} + \delta_{int}} \tag{6}$$

2.1. Validation with different codes (NZS 3404 and AISC 360)

Though a large amount efforts and studies that has been devoted for the calculation of the ultimate strength of the braces [50], most of the international building codes now use the empirical curves to calculate the ultimate strength of a column in the interest of simplicity and accuracy. In this section, the results of the proposed SCMA method (Eq.5 or Eq.6) is compared with both AISC 360 [51] and NZS 3404 [46] prescriptions just to validate the methodology. Note this section is concerning the conventional steel braces with prismatic section and the framework will be extended for self-centring brace in the next section.

In this manner, three steel structural shapes namely, SHS (Square Hollow Section), UC (Universal Column or IPB) and UB (Universal Beam or IPE) were opted. The slenderness ratio (λ) of the hypothetical brace was assumed to vary between zero and 300 while the end condition was assumed to be the ideal pin – pin. The steel material was assumed to be mild steel with yield stress of 340 Mpa and the elastic modulus of 200 GPa. The resultant ultimate forces calculated from Eq.5 or Eq.6 based on the SCMA were calibrated with the cross-section area and are plotted in Fig. 3 against different slenderness ratio.

As evident in Fig. 3, for the slender braces, the result of SCMA is matching the codes. However, for the stocky braces, the results of the SCMA were slightly overestimated. The reason can be attributed to two phenomena. The first reason is that the effect of residual stress is not included in the SCMA, which partially resulted in the overestimation. The second and more important reason is that the SCMA always gives
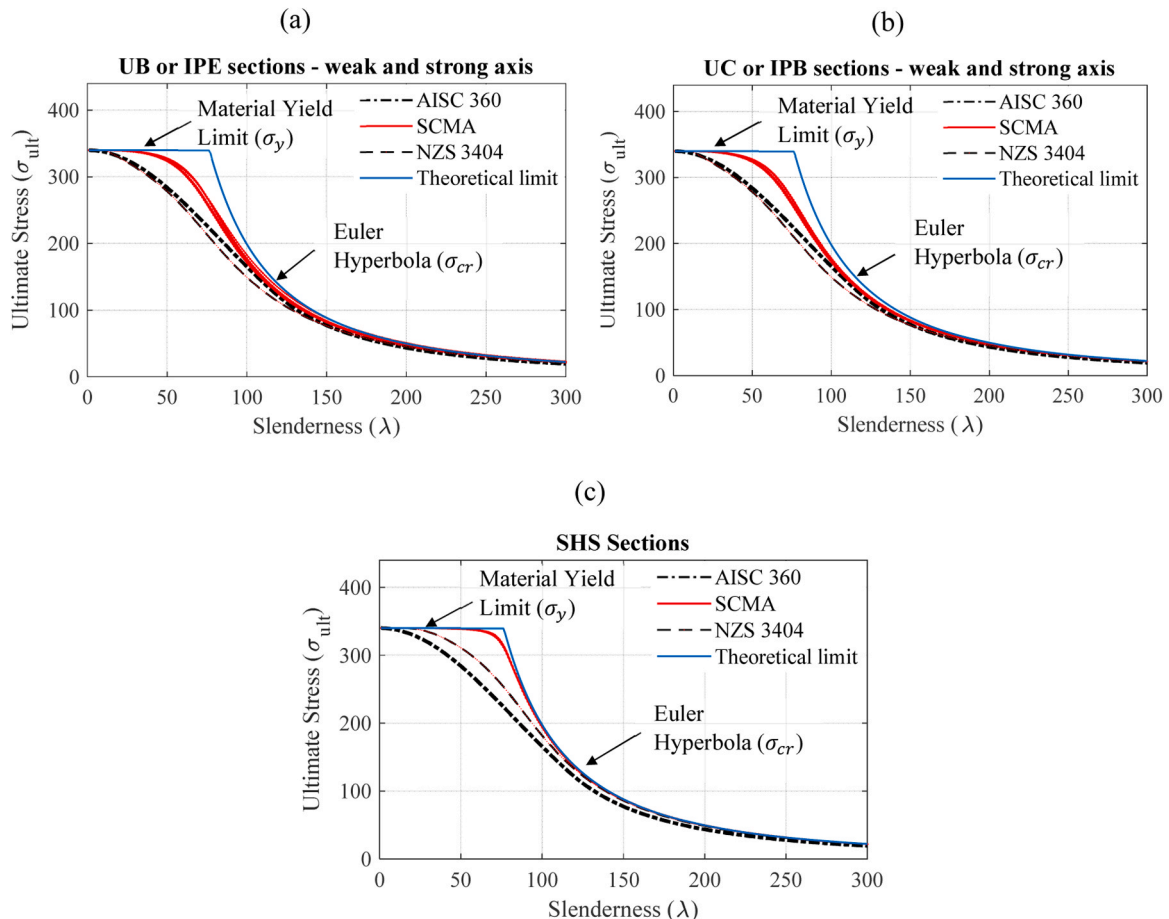
(a) (b)

(c)

Fig. 3. : Comparison among SCMA, AISC 360 and NZS3404 (a) UB section, (b) UC section and (c) SHS section.

the upper bound of the result (See chapter 6 [45] or [52]). Given Fig. 2, it can be seen that the intersection point (red dot) falls always above the real value (black dot) of ultimate capacity, which will result in the overestimation the capacity. This overestimation can be compensated with a calibration factor based on the slenderness [52].

3. Generalization of SCMA to self-centring RSFJ brace assembly

Self-centring brace in this study is composed of three components namely: (a) self-centring friction damper (RSFJ) [27,29,32,33,53] for which the performance is shown in Fig. 4, (b) brace body, which can be made of timber [27] or steel [54] and (c) Anti-buckling tubes.

As discussed, the SCMA method had two main steps. The first and foremost step is to approximate the elastic buckling load of the system from which the stiffness deterioration path (Eq.1) will be discovered. The second step is to calculate the ultimate strength curve of the system as a function of lateral displacement. The intersection between two diagrams will bring the approximate ultimate strength of the system. Accordingly, this section firstly deals with calculating the elastic buckling of the self-centring brace and then deals with calculating the ultimate strength function.

3.1. Stiffness deterioration curve

As shown in the first part of the paper, the elastic buckling of a pin-pin brace with a uniform prismatic section was $\pi^2 EI/L^2$. However, this is not necessarily valid for the self-centring brace along with which non-continuities may appear. In this regards, the stability model that has been developed for the RSFJ brace assembly with one non-continuity [27] has been extended here to be used for a system with two non-continuities (the proof is provided in the appendix). The elastic buckling load can be calculated using Eq.7:

$$P_{cr} = \alpha \frac{EI}{L^2} \tag{7}$$

where L is the total length of the brace, EI is the flexural rigidity of the brace body and parameter α is the minimum real positive root of Eq.8 (characteristic equation) and is expected to be less than π^2 if the first mode of buckling is considered:

$$f(\delta_1, \beta) = 2\alpha\sin\left(\sqrt{\alpha}\,(2\delta_1 - 1)\right) - \alpha\sin\left(\sqrt{\alpha}\,(4\delta_1 - 1)\right) + \alpha\sin\left(\sqrt{\alpha}\right) - 4\beta^2\sin\left(\sqrt{\alpha}\right) + 4\sqrt{\alpha}\beta\cos\left(\sqrt{\alpha}\,(2\delta_1 - 1)\right) - 4\sqrt{\alpha}\beta\cos\left(\sqrt{\alpha}\right) \tag{8}$$

in which δ_1 and β are the relative location (Fig. 5) and relative rotational stiffness of the non-continuity region, respectively and can be calculated using Eq.9 and Eq.10:
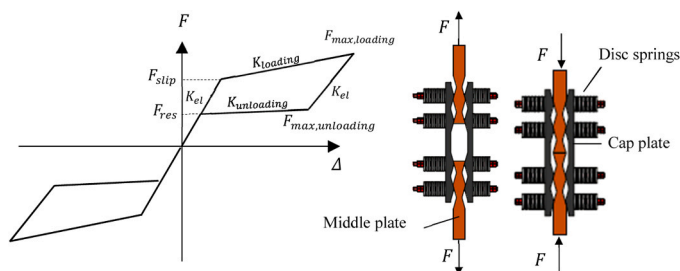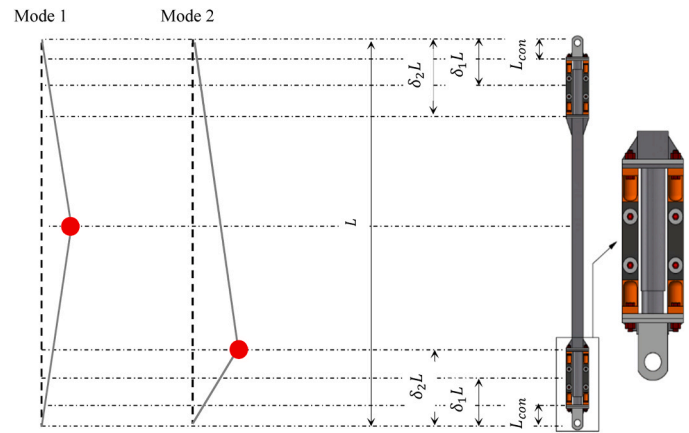

Fig. 5. different in-plane failure (mechanism) modes of the brace.

$$\delta_1 = \frac{0.5L_{RSFJ} + L_{con}}{L} \tag{9}$$

$$\beta = \frac{(K_{rot})_{ABT}L}{EI} \tag{10}$$

in which L_{con} is the distance between the pin and beginning of the damper as shown in Fig. 5, L_{RSFJ} is the length of damper and $(K_{rot})_{ABT}$ is the rotational stiffness of the non-continuity region, which is assumed to be only coming from ABT. This parameter can be simply derived using the method of virtual work [55]. The rotational stiffness of the ABT is illustrated in Eq.11 as:

$$(K_{rot})_{ABT} = \frac{2m.EI_{ABT}}{\delta_2 L} \tag{11}$$

in which

$$m = \frac{\delta_2}{[2(\delta_2 - \delta_1) + \beta_b(1 - 2\delta_2)]} \tag{12}$$

In the two above-mentioned equations, parameters β_b and δ_2 are the relative rigidity and relative length of ABT (Fig. 5):

$$\delta_2 = \frac{L_{RSFJ} + L_{con}}{L} \tag{13}$$

$$\beta_b = \frac{(EI)_{ABT}}{EI} \tag{14}$$

Once the elastic buckling load is recognized, the stiffness deterioration curve can be approximated using Eq.1 in which the initial imperfection is suggested to be:

$$\delta_0 = \frac{L}{1000} + \frac{L}{500} + \delta_{clearance} \tag{15}$$

in which the initial imperfection of the body is (L/1000), errection tolerance is L/500 and $\delta_{clearance}$ is the additional clearance in the gusset and ABTs. It should be mentioned that a parametric finite element study has been performed in [45] in order to validate this model.

Fig. 4. : Performance and deflected shape of RSFJ damper in tension and compression.

3.2. Strength deterioration curve

Fig. 5 shows the different possible in-plane failure mechanisms of the RSFJ brace. Note that the damper-brace in considered as fixed-fixed for out-of-plane behaviour and pined-pined for in-plane behaviour. Generally, there are two possible places for a plastic hinge to form in the system namely: (a) mid-span of the brace body (mode 1) because the second-order moment tends to be at the highest level at this section and (b) end of the brace body within the female section of the ABT (mode 2) because of the nonequality of ABT section and the brace body. It is worth noting that the first collapse mode is desired mainly because in the mode 2, the damper would be damaged due to the deformation compatibility between ABT and the damper. In this regard, the experimental destructive tests were mainly focused on the first mode. This will be further discussed in the following sections.

In order to calculated the strength deterioration curve of the system, the second-order plastic analysis using the virtual energy method is used. In case of both modes of collapse (Fig. 5), the plastic strain energy stored in the plastic hinge is:

$$U = \left(M_p\right)^{'} \times 2\theta \tag{16}$$

In which 2θ is the rotation in the plastic hinge, $\left(M_p\right)^{'}$ is the reduced plastic capacity of the section if there is any axial load. The work carried out as a result of axial deformation can be calculated as [47]:

$$T = PL(1 - \cos\theta) \tag{17}$$

By satisfying the balance of energy, the strict minimum of the potential energy [43,44,47], the ultimate strength can be derived:

$$\frac{d(U - T)}{d\theta} = 2\left(M_p\right)^{'} - PL\theta = 0 \tag{18}$$

If the axial loads (P) is brought in the left side the equation, the *strength* deterioration can be calculated as a function of lateral displacement (δ):
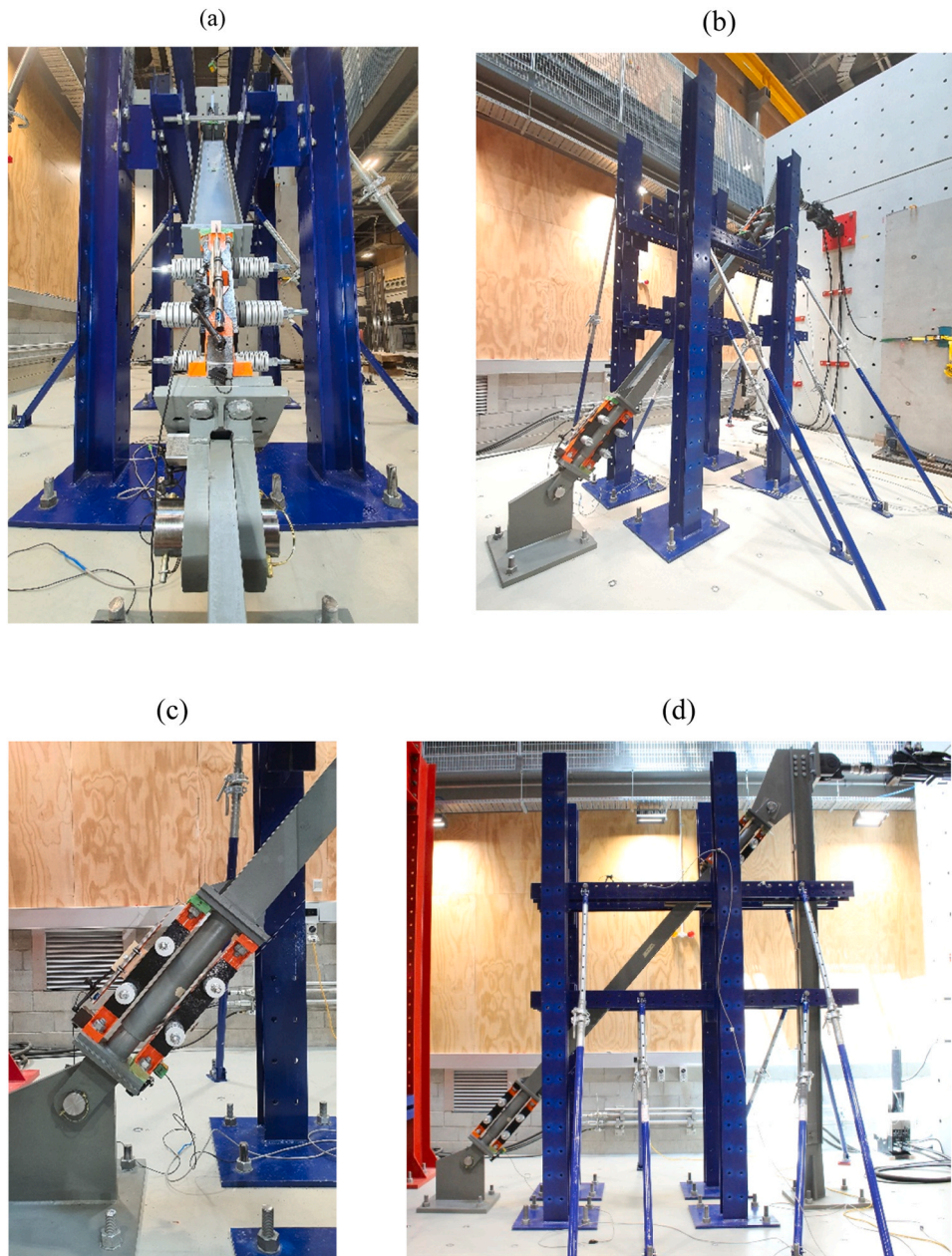
(a)

(b)

(c)

(d)

Fig. 6. : Test set for steel RSFJ brace: (a) isometric view, (b) front view, (c) side view-joint and (d) side view-brace.

$$P = \frac{(M_p)'}{\delta} \qquad (19)$$

Eq.19 will lead to Eq.2 if the mode 1 is considered but will lead to Eq.20 if mode 2 is considered:

$$P = \frac{(M_p)_{female}}{\delta} \qquad (20)$$

in which $(M_p)_{female}$ is the plastic capacity of the female section of the ABT without any reduction because no axial load is transferred by the ABT (telescopic configuration). Accordingly, the intersection point between the stiffness and strength deterioration curves when the mode 2 is considered can be estimated as:

$$\delta_{\text{int}_{female}} = 0.5(M_p)_{female}\left[\frac{1}{P_{cr}} + \sqrt{\left(\frac{1}{P_{cr}}\right)^2 + \frac{4\delta_0}{(M_p)_{female}.P_{cr}}}\right] \qquad (21)$$

Note that the intersection point for mode 1 was already illustrated in Eq.4 yet the elastic buckling load (P_{cr}) should be input from Eq.7. By having two intersection points (Eq.4 and Eq.21) from two failure modes, the associated ultimate strength of the RSFJ brace can be approximated using Eq.5 or Eq.6 and the lowest force obtained shall be considered as the system ultimate capacity.

4. Experimental validation

4.1. Test set up

A full-scale experimental test was performed at Auckland University of Technology laboratory for which the test set up is shown in Fig. 6. A total of 3 specimens (tabulated in Table1) were employed and the drawings are provided in Fig. 7. Each specimen had a 4466 mm length and was installed at an angle of 49.2 degree with respect to horizontal floor. Both brace bodies and the ABTs were manufactured using mild steel with nominal yield strength of 340 MPa and an elastic modulus of 200 GPa. Two locations along with the brace were considered for the dampers' installation in each of which two dampers were located. For the purpose of testing, a 250 kN MTS actuator with ± 125 mm stroke capacity was used. For the purpose of data acquisition two drew wires and two LVDTs (Linear Variable Differential Transformer) were used, which LVDTs were responsible to record the dampers axial movement, and drew wires were responsible to record the brace axial and lateral deformations, respectively. In this program, two of the specimens were supposed to be failed in the destructive tests while one specimen was designed to stay undamaged to study the dynamic behaviour of the brace.

4.2. Component testing of RSFJs

The RSFJ damper in this study was already tested experimentally by Authors [27]. However, in this study, the number of disc springs and their prestressing force (F_{pr}) have been changed to suit the test and reach the desired level of load at the desired level of displacement. There were four RSFJs in total for each brace specimen all of which had the same

characteristics in terms of flag-shape performance as reported in Table2. All of the RSFJs were tested according to the prescribed load protocol of AISC 341 for BRBs [27,32] shown in Fig. 8.a with a loading rate of 1 mm/s. The experimental results of the component testing are shown in Fig. 8.b.

4.3. Full-scale Testing

This section discusses the results of three brace specimens. In the first part of this section, the result of specimen SCB1 is discussed, which was designed to be undamaged during the testing program, and therefore, the main emphasis in this section is placed on the evaluation of the brace performance when it is subjected to a static and dynamic loading regime. In the second part of this section, the results of the destructive tests on the specimens SCB2 and SCB3 are discussed where the failure mode 1 was intended to be observed. The failure of the brace according to mode 2 was not investigated in this study mainly because it may have contributed to yielding the damper due to deformation compatibility. However, it should be also pointed that the failure according to the mode 2 was studied [27] but with the difference that the brace was not strengthened with ABT, and there was one weakened location along with the brace for the damper installation.

4.3.1. Reversed Cyclic Static and Dynamic test on SCB1

A full-scale reversed cyclic test in both static and dynamic manner was performed on the brace SCB1 designed to remain undamaged for the actuator capacity (250 kN). Validation with the dynamic test is a requirement for certifying any damper performance according to ASCE 7 [56] mostly because it tends to simulate the real case at the time a seismic event and observe the possible behavioural change of the friction damper (such as coefficient of friction, repeatability and damping) [57]. Therefore, this section is devoted to the experimental study of the damper performance subjected to different protocols with different excitation velocity.

Based on the literature [27,32,58,59], evaluation of a self-centring brace performance against the combined load protocol of AISC 341 - for Buckling-Restrained Frame [60] - and the dynamic load protocol of ASCE 7–13 for dampers [56] would suffice to approve the brace performance [27,32,59]. For this purpose, the brace SCB1 was firstly subjected to a reversed static cyclic loading protocol up to 2.5% drift with constant loading rate of 1 mm/s and repetition of two for each amplitude as shown in Fig. 9.a. The result of the reversed quasi-static cyclic test is shown in Fig. 9.b.

After conducting the quasi-static test, the specimen SCB1 was subjected to two sinusoidal-shaped dynamic load protocols (Fig. 9.c and Fig. 9.e) up to 2% drift with 0.25 Hz (equivalent to maximum velocity of 40 mm/s) and 0.4 Hz (equivalent to maximum velocity of 64 mm/s) frequency in which the last cycle (40 mm -) was repeated for five times as per requirement of ASCE 7–13 [56]. The results of these two tests are shown in Fig. 9.d and Fig. 9.f. As can be observed, the brace performance in all three experiments was in accordance with the analytical predictions [27] and more importantly, its behaviour was unaffected due to dynamic loading regime.

Table 1
Testing Plan and Specimens' information.

Specimens	Brace body section	Anti-buckling Tube				L_{RSFJ} (mm)	L (mm)	δ_1L (mm)	δ_2L (mm)	Expected mode of failure
		Female		Male						
		Outer diameter (mm)	Inner diameter (mm)	Outer diameter (mm)	Inner diameter (mm)					
SCB1	250 UB	114	105.3	101.6	91.6	633	4466	526.5	843	Undamaged
SCB2	180 UB	114	105.3	101.6	91.6					Brace Body
SCB3	150UB	88.9	78.9	76.1	66.1					Brace Body

(a)

SCB1:

SCB2:
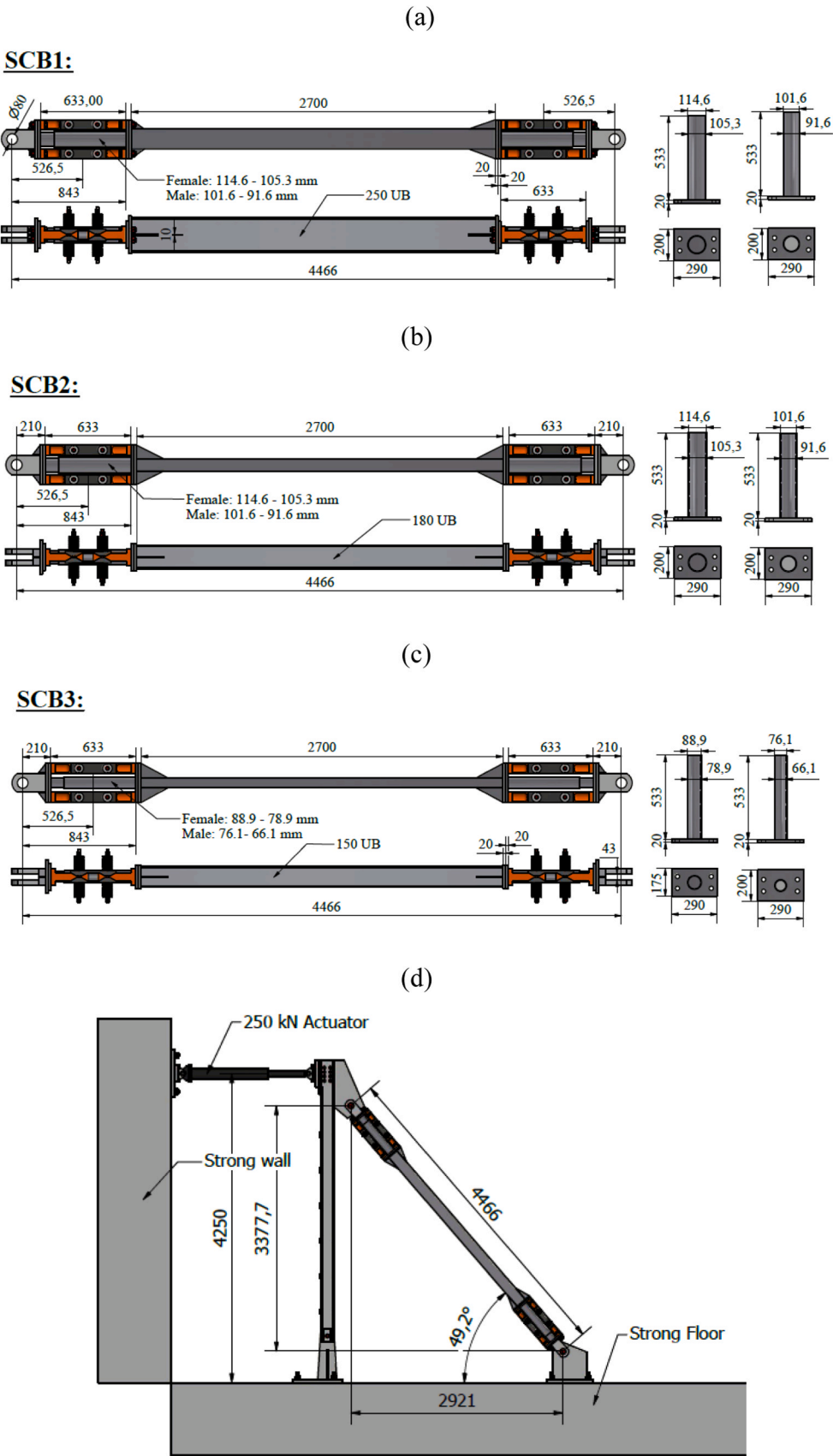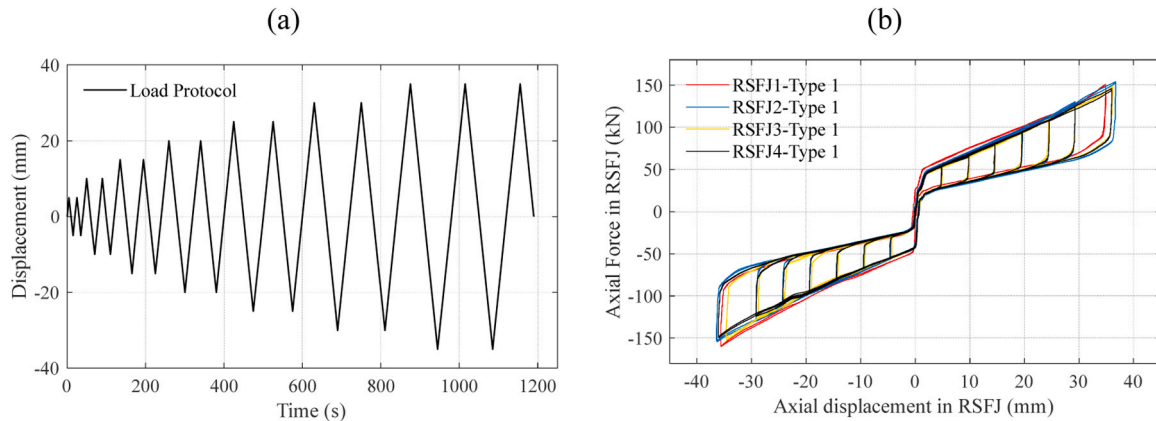
(b)

SCB3:

(c)

(d)

Fig. 7. : Specimens and set up dimensions: (a) SCB1, (b) SCB2, (c) SCB3, (d) Test set up dimensions.

Table 2
Damper characteristics for different specimens (Refer to the Fig. 4 for damper hysteresis parameters).

Specimens	n_d	bolt prestressing F_{pr} (kN)	Slip force F_{slip} (kN)	Residual force $F_{residual}$ (kN)	Ultimate force $F_{max,loading}$ (kN)	Unloading force $F_{max,unloading}$ (kN)
SCB1 SCB2 SCB3	14	36	56.7	24.7	146.6	63.8

Fig. 8. : Experimental results of the component testing of the dampers: (a) displacement load protocol, (b) Hysteric performance of RSFJs subjected to the load protocol.

4.3.2. Destructive Monotonic test on Specimen SCB2 and SCB3

Fig. 10.a and Fig. 10.b show the result of monotonic test on specimen SCB2 with 180 UB 22 as for the brace body. The elastic buckling of this specimen according to the procedure explained in Section3.2 was calculated to be 104.3 kN, to which the stiffness deterioration curve (green line) was approaching. According to Fig. 10.a, it can be observed that the ultimate strength of the brace should have been around 100 kN based on the SCMA method, which is the intersection between the green and purple curves. However, the ultimate strength was observed to be 200 kN based on experimental data. After further scrutiny of the test, it was discovered that the specimen was tightly gripped between two lateral supports as shown in Fig. 10.c. The lateral supports, buttressed with diagonal props, were originally used with the intention of limiting the out-of-plane displacement of the setup; however, they unfortunately contributed to performing as an unintentional intermediate constraint and as a result, providing a shorter effective length for buckling. Further evidence was that the plastic hinge was formed in the brace body with an offset from the midspan (shown in Fig. 10.d), the location it is was supposed to be formed. In order to correct the prediction of the proposed method, the length of the brace was replaced with the distance between the end pin and the intermediate constraint. The modified buckling load was approximated to be 192 kN (shown in Fig. 10.a with blue line). This have resulted in the predicted ultimate strength of 184 kN (the intersection between blue and purple curves).

Fig. 10.b shows the recorded axial load in the brace against the measured axial displacement. As can be seen, the dash-dotted line is the ideal flag-shape performance of the brace, which was not accomplished by the specimen due to the premature inelastic buckling of the brace. In this specimen, the failure occurred in the after-slip phase, but in the next specimen SCB3, the inelastic buckling occurred in the before-slip phase.

The problem of additional intermediate constraint was tackled for the test on specimen SCB3 and the ultimate strength of the brace was observed to be nearly 71.5 kN. According to Fig. 11.a, it can be observed that the ultimate strength of the brace was estimated 55.7 kN, the intersection between blue and purple curves. As shown in Fig. 11.b, the specimen SCB3 experienced a premature failure and buckled inelastically even before the slippage of the dampers in the brace (activation force shown in Fig. 11.b).

From both test results on SCB2 and SCB3, the importance of having a framework to quantify the ultimate load of the brace can be highlighted. In both cases, the specimens were not able to reach the same capacity as their design target and buckled inelastically.

5. Further discussions

5.1. Desirable mode

As discussed in Section 3, two possible failure modes may exist for the self-centring brace. The first scenario was that the plastic hinge forms at the mid-span of the brace and within the brace body. This is more probable when the relative stiffness (β_b) is considerable [45,52]. The second one is that the plastic hinge forms within the damper location and in the female part of the ABT. This scenario is more probable when the relative rigidity (β_b) of the ABT to brace body is small [45,52]. The first case seems to be desirable and recommended to be governed in the design process mainly because if the plastic hinge forms within the ABT, it indicates that the damper would be damaged, and the brace may not resist any further inelastic load cycles either in the main event or aftershocks. The next benefit is that if the brace body is attached to the damper using the bolted connections, like the braces used in this paper (Fig. 7), it can be easily replaced in case of being damaged during a seismic event beyond the design level.

5.2. Additional shear

Normally shear force in the braces is negligible since originating from the second-order actions ($p - \Delta$), but they can be critical in some cases (designing connections, welding and so on) and discussed here accordingly. Assuming that the plastic hinge is formed at the mid-span of the brace, the deflected shape at the ultimate limit state would be:

According to Fig. 12 and assuming that the deformations are of small magnitude ($\sin\theta \sim \tan\theta \sim \theta \& \cos\theta \sim 1$), the shear force due to $p - \Delta$ and formation of plastic hinge can be approximated with the vertical component of the ultimate load as "$P'_{ult}\tan\theta$ or $P'_{ult}\theta$". It should be pointed out that the "P'_{ult}" and "δ'_{int}" are the modified ultimate load and
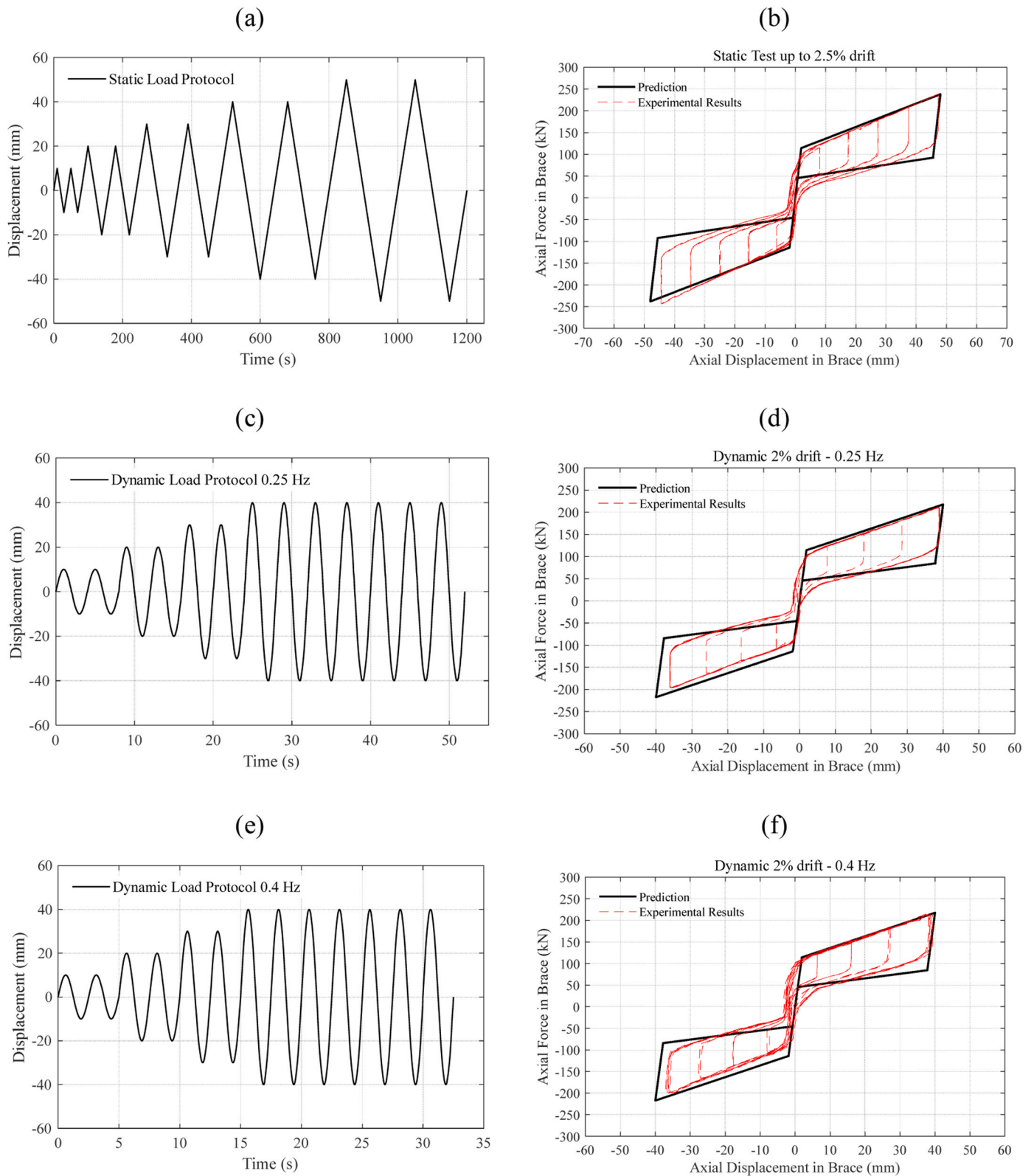
Fig. 9. : Experimental results of the specimen SCB1: (a, b) Load protocol and hysteresis response for the static test, (c, d) Load protocol and hysteresis response for the dynamic test 0.25 Hz, (e, f) Load protocol and hysteresis response for the dynamic test 0.4 Hz.

intersection point with respect to the material overstrength. In other word, the strength deterioration curve should be multiplied by the material overstrength factor $R_y(M_p)^{'}$, and then the ultimate load and intersection point should be recalculated and relocated. The stiffness

deterioration curve does not need to be modified as it is independent from the material yielding limit. This modification originates from the well-known capacity design concept. If the initial imperfection (L/1000) of the body, errection tolerance (L/500) and clearance in the connection is also considered, the additional shear force due to second-order and
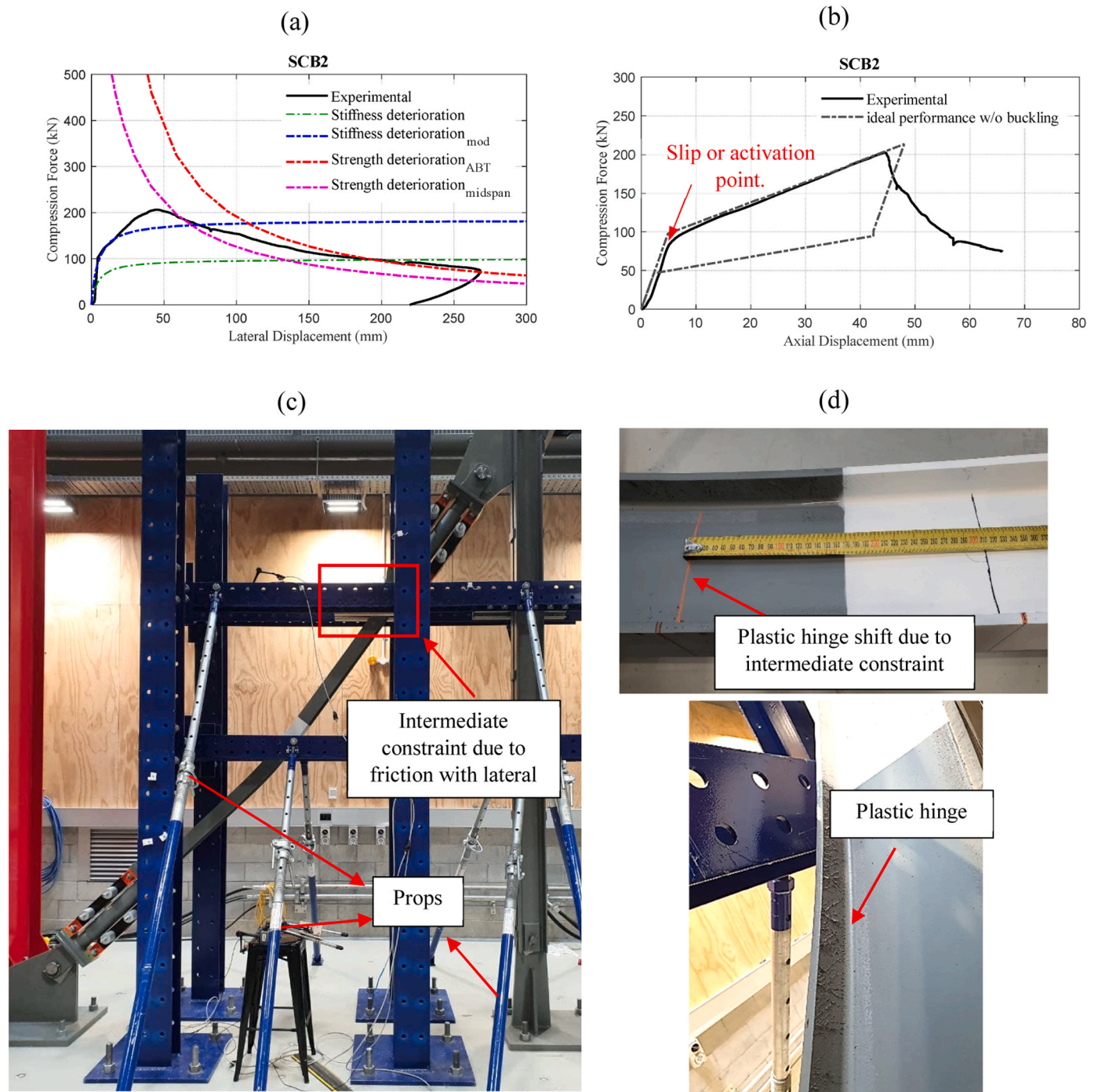
Fig. 10. : Experimental results of specimen SCB2: (a) axial load Vs lateral deflection, (b) axial load Vs axial displacement, (c) deformed shape of tested brace and (d) plastic hinge formation.

plastic hinge formation can be calculated using Eq.22:

$$V_u = P'_{ult}\left(\frac{2\delta'_{int}}{L} + \frac{1}{1000} + \frac{1}{500} + \theta_{clearance}\right) \geq 0.004P'_{ult} \qquad (22)$$

where $\theta_{clearance}$ is the additional initial rotation due possible clearance in the connections (gusset plate and ABT). The value of the shear force is also recommended to be more than $0.004P'_{ult}$, suggested by the AISC 360 [51] – Appendix 6 (requirement for compressive member bracing). In this regard, all elements of the brace – connections, bolts, welding and etc – should be checked to be able to resist this additional shear.

5.3. End plate design

Another point that should be considered in the seismic design of the RSFJ brace is the design of the ABT's end plates as shown in Fig. 13. This plate should possess the sufficient strength so that the performance of the brace is not disrupted because of the local yielding of the plate. In case that the governing failure mode is the mode 2 (plastic hinge forms within the ABT), then the endplate should be designed in a way to be capable of accommodating the factored plastic capacity of the ABT (plastic capacity including the material overstrength). However, if the governing failure mode is the first mode (plastic hinge forms within the brace body), then the endplate can be designed for the existing moment
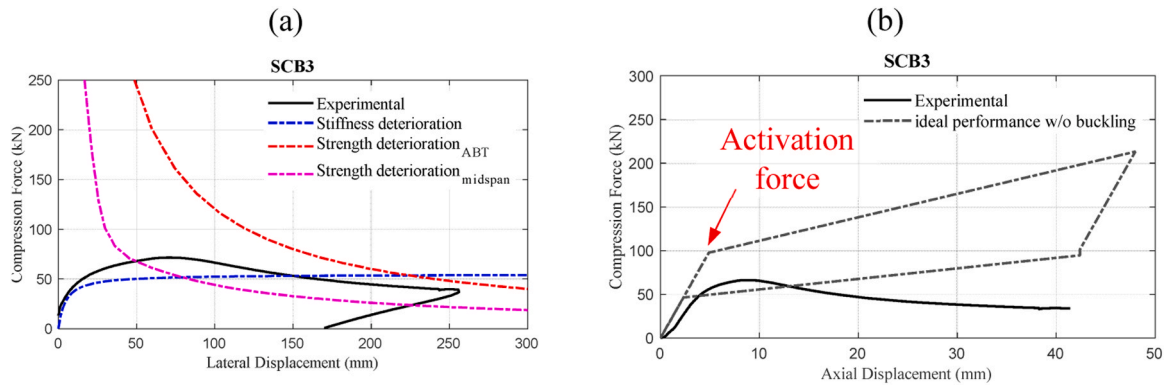
(a)

(b)

Fig. 11. : Experimental results of specimen SCB3: (a) axial load Vs lateral deflection and (b) axial load Vs axial displacement.
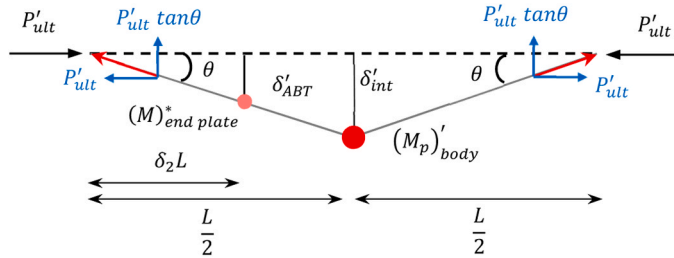

Fig. 12. : Deformed shape of the brace at the time of mechanism formation.
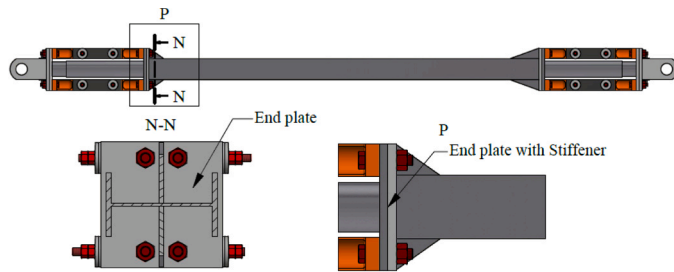

Fig. 13. End plate.

demand as shown in Eq.23 and Fig. 12. This value tends to be less demanding as compared to the first case:

$$(M)^*_{end\ plate} = P'_{ult}\delta'_{ABT} \sim 2P'_{ult}(\delta_2\delta'_{int}) \tag{23}$$

5.4. Design flowchart

Fig. 14 summarizes the whole process of RSFJ brace design (for compression) in six consecutive steps. The process initiates with calculating the elastic buckling load of the system (P_{cr}). Though a procedure was developed in this study (Section 3.2) to calculate the elastic buckling load, any other well-known methods or simulation techniques with the finite element software can be recruited at step 1 to determine the elastic buckling load. At step 2, the pure axial capacity (squash strength) P_n is determined, which along with the critical load P_{cr} will be input into the intersection formulations to figure out at what lateral deflection (δ_{int}), the plastic hinges may form. The process continues in step 4 with calculating the ultimate loads associated with each failure mode where the minimum of them shall be taken as the final ultimate load, and the associated mode is called the governing failure mode. While in this step, it should be also made sure that the failure mode is the first mode; otherwise, a stronger ABT should be opted, and the previous steps should be repeated. In step 5, the brace demand must be checked against
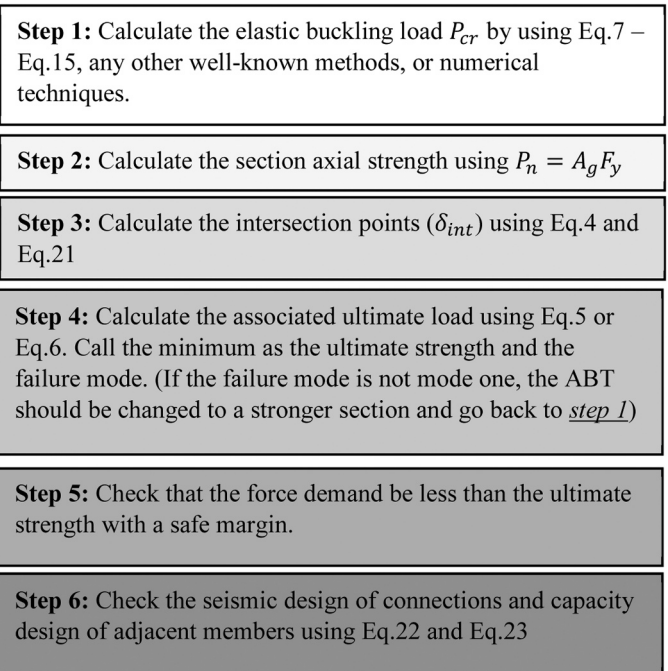
Step 1: Calculate the elastic buckling load P_{cr} by using Eq.7 – Eq.15, any other well-known methods, or numerical techniques.

Step 2: Calculate the section axial strength using $P_n = A_gF_y$

Step 3: Calculate the intersection points (δ_{int}) using Eq.4 and Eq.21

Step 4: Calculate the associated ultimate load using Eq.5 or Eq.6. Call the minimum as the ultimate strength and the failure mode. (If the failure mode is not mode one, the ABT should be changed to a stronger section and go back to *step 1*)

Step 5: Check that the force demand be less than the ultimate strength with a safe margin.

Step 6: Check the seismic design of connections and capacity design of adjacent members using Eq.22 and Eq.23

Fig. 14. The proposed damper-brace design steps.

the ultimate load to be less with a safe margin. The process ends with the capacity design of the connections and adjacent members. Readers are encouraged to see [52] for a solved real-world design example to grasp a better understanding of the step-by-step procedure.

6. Summary and concluding remarks

Previous studies on the RSFJ steel brace demonstrated that the compression capacity of the brace might be of low magnitude due to rotational flexibility of the damper for which a telescopic mechanism was suggested to be put in parallel to the dampers to increase their rotational stiffness. Doing that successfully increased the elastic buckling load of the system, yet the ultimate strength and collapse mode of this system was not clearly investigated. In this manner, a framework was proposed to predict the possible failure loads and collapse mechanism of the RSFJ brace in compression. Some of the outcomes and conclusions from this study is listed below:

- A simplified approach (SCMA) based on the second-order plastic analysis of system was developed by which the inelastic buckling capacity of the self-centring system as well as its failure mode can be

predicted. It should be pointed out that while the experimental demonstration was limited to the RSFJ brace assembly, this method is applicable to other self-centring systems or new compressive members given its underlying basis. In this respect, further investigation and international effort is required.

- Both quasi-static and dynamic reversed cyclic tests were conducted on the brace specimens using the code-compliant loading protocols, and it was observed that dynamic behaviour of the system was not affected by the high velocity of loading.
- Two destructive monotonic tests were performed in order to validate the proposed method for inelastic buckling strength quantification.
- It was discussed that the desired failure mode is when the plastic hinge forms within the brace body so that the damper performance does not get disrupted. Accordingly, the seismic design requirements to design the connections and protected elements of the brace were discussed.

- Finally, a step-by-step procedure was provided so that an engineer can design the self-centring brace in a straightforward manner.

Statement

Acknowledgment

Appendix. : proof of the characteristic equation

In order to calculate the characteristic equation of the system shown in Figure ſ0.zd, the deflected shape of each segments (three in total) can be assumed as the following three expressions (Eqs. A1-A3) having variable coefficient C_i, B_i and E_i ($i = 1, 2, 3$). For the simplicity of the solution, the normalized length is considered in the process:

$$y_1 = C_1 \sin\left(\sqrt{\alpha}\,x\right) + C_2 \cos\left(\sqrt{\alpha}\,x\right) + C_3 x + C_4, 0 \leq \frac{x}{L} < a \tag{A1}$$

$$y_2 = B_1 \sin\left(\sqrt{\alpha}\,x\right) + B_2 \cos\left(\sqrt{\alpha}\,x\right) + B_3 x + B_4, a \leq \frac{x}{L} < b \tag{A2}$$

$$y_3 = E_1 \sin\left(\sqrt{\alpha}\,x\right) + E_2 \cos\left(\sqrt{\alpha}\,x\right) + E_3 x + E_4, b \leq \frac{x}{L} < 1 \tag{A3}$$
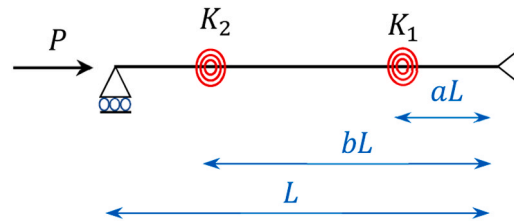

Fig. ſ0.1. Mathematical model.

.

Each boundary condition of the system will put a constraint on the deflection expression. Therefore, all of them should be met based on the assumed deflection shape at the same time. The first set of boundary conditions is the continuity of the shape necessitating to satisfy:

$y_1(0) = 0$

$y_1(a) = y_2(a)$

$y_3(1) = 0$

$y_2(b) = y_3(b)$ (A4)

The second set is the continuity of the curvature and zero bending at pin supports, which requires:

$\dfrac{d^2 y_1}{dx^2}(0) = 0$

$\dfrac{d^2 y_3}{dx^2}(1) = 0$

$\dfrac{d^2 y_1}{dx^2}(a) = \dfrac{d^2 y_2}{dx^2}(a)$

$\dfrac{d^2 y_2}{dx^2}(b) = \dfrac{d^2 y_3}{dx^2}(b)$ (A5)

The third set of boundary condition is the continuity of the shear at the locations where the rotational springs are installed, which necessitates:

$$\frac{d^3 y_1}{dx^3}(a) + \alpha \frac{dy_1}{dx}(a) = \frac{d^3 y_2}{dx^3}(a) + \alpha \frac{dy_2}{dx}(a)$$

$$\frac{d^3 y_2}{dx^3}(b) + \alpha \frac{dy_2}{dx}(b) = \frac{d^3 y_3}{dx^3}(b) + \alpha \frac{dy_3}{dx}(b) \tag{A6}$$

The last one is the deformation compatibility and equilibrium at the location of rotational springs, which brings:

$$\frac{d^2 y_1}{dx^2}(a) = k_1 \left(\frac{dy_2}{dx} - \frac{dy_1}{dx} \right)(a)$$

$$\frac{d^2 y_2}{dx^2}(b) = k_2 \left(\frac{dy_2}{dx} - \frac{dy_1}{dx} \right)(b) \tag{A7}$$

in which

$$k_1 = \frac{K_1 L}{EI}$$

$$k_2 = \frac{K_2 L}{EI} \tag{A8}$$

In order that all of the above-mentioned equation are satisfied at the same time, the determinant of the coefficients of all equations should be zero, which yields the characteristic equation as following:

$$f(a, k_1, k_2) = 2\alpha \sin\left(\sqrt{\alpha}(2a-1)\right) - \alpha \sin\left(\sqrt{\alpha}(4a-1)\right) + \alpha \sin\left(\sqrt{\alpha}\right) - 4k_1 k_2 \sin\left(\sqrt{\alpha}\right) + 2\sqrt{\alpha}(k_1+k_2)\cos\left(\sqrt{\alpha}(2a-1)\right) - 2\sqrt{\alpha}(k_1+k_2)\cos\left(\sqrt{\alpha}\right) \tag{A9}$$

In Eq.13.21, if $k_1 = k_2 = \beta$ and $a = \delta$

$$f(\delta, k) = 2\alpha \sin\left(\sqrt{\alpha}(2\delta-1)\right) - \alpha \sin\left(\sqrt{\alpha}(4\delta-1)\right) + \alpha \sin\left(\sqrt{\alpha}\right) - 4k^2 \sin\left(\sqrt{\alpha}\right) + 4\sqrt{\alpha}k\cos\left(\sqrt{\alpha}(2\delta-1)\right) - 4\sqrt{\alpha}k\cos\left(\sqrt{\alpha}\right) \tag{A10}$$

The real root of the results of Eq. A10 should be input in Eq. A11 to determine the Euler load or elastic buckling load of the system:

$$P_{cr} = \alpha \frac{EI}{L^2} \tag{A11}$$

where α should be bounded for first mode as:

$$\alpha \in \left(0, \pi^2\right) \tag{A12}$$

For the second mode of elastic buckling, α should be bounded:

$$\alpha \in \left(\pi^2, 4\pi^2\right) \tag{A13}$$

References

[1] Chancellor NB, et al. Self-centering seismic lateral force resisting systems: High performance structures for the city of tomorrow. Buildings 2014;4(3):520–48.

[2] Priestley MN, et al. Preliminary results and conclusions from the PRESSS five-story precast concrete test building. PCI J 1999;44(6):42–67.

[3] Christopoulos C, et al. Self-centering energy dissipative bracing system for the seismic resistance of structures: development and validation. J Struct Eng 2008; 134(1):96–107.

[4] Erochko J, Christopoulos C, Tremblay R. Design and testing of an enhanced-elongation telescoping self-centering energy-dissipative brace. J Struct Eng 2015; 141(6):04014163.

[5] McCormick J, et al. Seismic assessment of concentrically braced steel frames with shape memory alloy braces. J Struct Eng 2007;133(6):862–70.

[6] Zhang A, et al. Performance study of self-centering steel frame with intermediate columns containing friction dampers. Eng Struct 2019;186:382–98.

[7] Eatherton MR, Fahnestock LA, Miller DJ. Computational study of self-centering buckling-restrained braced frame seismic performance. Earthq Eng Struct Dyn 2014;43(13):1897–914.

[8] Qiu C, Du X. Seismic performance of multistory CBFs with novel recentering energy dissipative braces. J Constr Steel Res 2019:105864.

[9] Issa AS, Alam MS. Seismic performance of a novel single and double spring-based piston bracing. J Struct Eng 2018;145(2):04018261.

[10] Qing Y, et al. Seismic responses of multistory buildings with self-centering buckling-restrained braces: influence of the pretension force. Eng Struct 2021;238: 112249.

[11] Hadad AA, Shahrooz BM, Fortney PJ. Innovative resilient steel braced frame with Belleville disk and shape memory alloy assemblies. Eng Struct 2021;237:112166.

[12] Xu L, Xie X, Li Z. Seismic behavior and design approach of variable-damping self-centering braced frame. J Struct Eng 2021;147(6):05021001.

[13] Hu S, Wang W, Qu B. Self-centering companion spines with friction spring dampers: validation test and direct displacement-based design. Eng Struct 2021; 238:112191.

[14] Hu S, et al. Development and validation test of a novel Self-centering Energy-absorbing Dual Rocking Core (SEDRC) system for seismic resilience. Eng Struct 2020;211:110424.

[15] Baktash P, Marsh C, Pall A. Seismic tests on a model shear wall with friction joints. Can J Civ Eng 1983;10(1):52–9.

[16] Pall AS, Marsh C, Fazio P. Friction joints for seismic control of large panel structures. J Prestress Concr Inst 1980;25(6):38–61.

[17] Popov EP, Grigorian CE, Yang T-S. Developments in seismic structural analysis and design. Eng Struct 1995;17(3):187–97.

[18] Clifton, G.C., Semi-rigid joints for moment-resisting steel framed seismic-resisting systems. 2005, ResearchSpace@ Auckland.

[19] Nims DK, Richter PJ, Bachman RE. The use of the energy dissipating restraint for seismic hazard mitigation. Earthq Spectra 1993;9(3):467–89.

[20] Filiatrault A, Tremblay R, Kar R. Performance evaluation of friction spring seismic damper. J Struct Eng 2000;126(4):491–9.

[21] Wang W, et al. Self-centering friction spring dampers for seismic resilience. Earthq Eng Struct Dyn 2019;48(9):1045–65.

[22] Khoo H-H, et al. Development of the self-centering Sliding Hinge Joint with friction ring springs. J Constr Steel Res 2012;78:201–11.

[23] Jaisee S, Yue F, Ooi YH. A state-of-the-art review on passive friction dampers and their applications. Eng Struct 2021;235:112022.

[24] Javidan MM, Kim J. Seismic retrofit of soft-first-story structures using rotational friction dampers. J Struct Eng 2019;145(12):04019162.

[25] Javidan MM, Kim J. Experimental and numerical sensitivity assessment of viscoelasticity for polymer composite materials. Sci Rep 2020;10(1):1–9.

[26] Zarnani, P. and P. Quenneville, *A resilient slip friction joint.* Patent No. WO2016185432A1, NZ IP Office, 2015.

[27] Yousef-beik SMM, et al. Experimental study on cyclic performance of a damage-free brace with self-centering connection. J Struct Eng 2021;147(1):04020299.
[28] Yousef-beik SMM, et al. Seismic performance improvement of conventional timber brace using re-centring friction connection. Structures 2020;26:958–68.
[29] Yousef-beik SMM, et al. A new self-centering brace with zero secondary stiffness using elastic buckling. J Constr Steel Res 2020;169:106035.
[30] Hashemi A, et al. Seismic strengthening of conventional timber structures using resilient braces. Structures. Elsevier; 2021.
[31] Yousef-beik SMM, et al. Effect of second-order actions on the performance of resilient slip friction joints: Analytical and experimental investigation. Structures. Elsevier,; 2021.
[32] Bagheri H, et al. A new self-centering tension-only brace using resilient slip friction joint: experimental tests and numerical analysis. J Struct Eng 2020.
[33] Bagheri H, et al. The resilient slip friction joint tension-only brace beyond its ultimate level. J Constr Steel Res 2020;172:106225.
[34] Darani, F., et al., Application of new resilient slip friction joint for seismic damage avoidance design of rocking concrete shear walls. 2018.
[35] Hashemi A, et al. Enhanced seismic performance of timber structures using resilient connections: full-scale testing and design procedure. J Struct Eng 2020; 146(9):04020180.
[36] Sahami, K., P. Zarnani, and P. Quenneville, Introducing a low damage system incorporating rocking braced frame and resilient slip friction joint as a shear key. 2020.
[37] Veismoradi S, et al. Seismic retrofitting of RC-frames using resilient slip friction joint toggle-bracing system. NZSEE Conf 2020.
[38] Veismoradi S, et al. Seismic strengthening of deficient RC frames using self-centering friction haunches. Eng Struct 2021;248:113261.
[39] Veismoradi S, Zarnani P, Quenneville P. Development of self-centring rotational slip friction joint: a novel damage-free damper with large deflections. Pac Conf Earthq Eng (PCEE) NZ Soc Earthq Eng (NZSEE), Auckl, NZ 2019.
[40] Veismoradi S, et al. Development and parametric study of a new self-centering rotational friction damper. Eng Struct 2021;235:112097.
[41] Yousef-beik SMM, et al. Lateral instability of self-centring braces: buckling in loading and unloading. Pac Conf Earthq Eng 2019.
[42] Xu L-H, et al. Hysteretic behavior and failure mechanism of an assembled self-centering brace. Bull Earthq Eng 2019;17(6):3573–92.
[43] Takeuchi T, et al. Out-of-plane stability of buckling-restrained braces including moment transfer capacity. Earthq Eng Struct Dyn 2014;43(6):851–69.
[44] Takeuchi T, Matsui R, Mihara S. Out-of-plane stability assessment of buckling-restrained braces including connections with chevron configuration. Earthq Eng Struct Dyn 2016;45(12):1895–917.
[45] Yousef-Beik SMM. Development of a New Self-Centring Low-damage Bracing System for Earthquake Resistance Using Resilient Slip Friction Joints (RSFJ), in Department of Built Environment Engineering. Auckland University of Technology; 2021.
[46] 3404, N., NZS 3404 Parts 1 & 2:1997 "Steel Structures Standard", Standards New Zealand. 1997: New.
[47] Bažant ZP, Cedolin L. Stability of structures: elastic, inelastic, fracture and damage theories. World Scientific; 2010.
[48] Newell JD, Uang C-M. Cyclic behavior of steel wide-flange columns subjected to large drift. J Struct Eng 2008;134(8):1334–42.
[49] Bruneau M, Uang C-M, Sabelli SR. Ductile design of steel structures. McGraw Hill Professional; 2011.
[50] Ziemian RD. Guide to stability design criteria for metal structures. John Wiley & Sons; 2010.
[51] 360–16, A., AISC 360–16 Specification for Structural Steel Buildings 2016: Chicago, IL.
[52] Yousef-Beik, S.M.M., et al., Design of RSFJ Self-centring Brace for Ultimate Limit State in NZSEE 2021. 2021: Christchurch, New Zealand.
[53] Yousef-beik, S.M.M., et al., Damage-avoidance timber brace using a self-centring friction damper in Pacific Conference on Eathquake Engineering. 2019: Auckland, New Zealand.
[54] Hashemi A, et al. Seismic performance of a damage avoidance self-centring brace with collapse prevention mechanism. J Constr Steel Res 2019;155:273–85.
[55] Hibbeler RC, Kiang T. Structural analysis. Pearson Prentice Hall Upper Saddle River; 2015.
[56] Standard A. ASCE/SEI, Minimum design loads for buildings and other structures. American-Society-of-Civil-Engineers,; 2013.
[57] Christopoulos C, Filiatrault A, Bertero VV. Principles of passive supplemental damping and seismic isolation, Vol. 133. Italy: Iuss press Pavia,; 2006.
[58] Erochko J, Christopoulos C, Tremblay R. Design, testing, and detailed component modeling of a high-capacity self-centering energy-dissipative brace. J Struct Eng 2014;141(8):04014193.
[59] Erochko J, Christopoulos C, Tremblay R. Design and testing of an enhanced-elongation telescoping self-centering energy-dissipative brace. J Struct Eng 2014; 141(6):04014163.
[60] AISC:341, AISC 341–10, Seismic Provisions for Structural Steel Buildings. Chicago, IL: American Institute of Steel Construction, 2010.